

Supporting Information

Construction of hierarchical carbon nanotube/MXene membrane with distinct fusiform channels for efficient molecular separation

Mingmei Ding,^{ab} Hang Xu,^{a} Wei Chen,^a Qing Kong,^a Tao Lin,^a Hui Tao,^a Kai Zhang,^c Qin Liu,^{bd} Kaisong Zhang,^d Zongli Xie^{b*}*

^a *Ministry of Education Key Laboratory of Integrated Regulation and Resource Development on Shallow Lakes, College of Environment, Hohai University, Nanjing 210098, China.*

^b *CSIRO Manufacturing, Private Bag 10, Clayton South, Vic. 3169, Australia.*

^c *State Key Laboratory of Environmental Aquatic Chemistry, Key Laboratory of Drinking Water Science and Technology, Research Center for Eco-Environmental Sciences, Chinese Academy of Sciences, Beijing, 100085, China*

^d *Institute of Urban Environment Chinese Academy of Sciences, Xiamen 361021, P.R. China.*

**Email: xuhang810826@163.com, zongli.xie@csiro.au.*

Detailed calculation methods

Calculation of hydrodynamic resistance of Membranes: A typical resistance model, where the resistance of the skin layer, R_{skin} , is an inherent property of the thin film of the substrate membrane, is employed for the hydrodynamic resistance calculations. The pure MXene and CNT-MX selective layer are first assumed to be the skin layers of the Nylon membrane before their hydrodynamic resistance are calculated using Equation S1:

$$R_{skin} = \frac{\Delta\pi_{skin}}{J_v\eta} = \frac{1}{\eta P} \quad (S1)$$

where skin (bar) is the transmembrane osmotic pressure difference across the skin layer, J_v ($\text{Lm}^{-2}\text{h}^{-1}$) is the water flux, η (m^2/s) is the viscosity of water and P ($\text{Lm}^{-2}\text{h}^{-1}\text{bar}^{-1}$) is the water permeance of the membrane¹. By substituting the water permeability coefficients obtained from Figure 5a, the hydrodynamic resistances exerted by the CNT-MX membranes, $R_{\text{CNT-MX}}$, are obtained and normalized against the resistance of the pure MXene membrane, R_{MXene} .

Calculation of the permeation parameter (K'): The Darcy's law states the liquid flow mechanism in porous media, and the permeate flux through membrane can be calculated by the following Equation S2.^{2,3}

$$Q = \frac{KATMP}{\mu R} \quad (S2)$$

where Q (L/h) is the flux, K is the proportionality coefficient, $A(\text{m}^2)$ is membrane area, $\text{TMP}(\text{bar})$ is the transmembrane pressure, μ ($\text{mPa}\cdot\text{s}$) is the viscosity of fluid, and R (m) is transport resistance. In our experiment, the water permeance P ($\text{Lm}^{-2}\text{h}^{-1}\text{bar}^{-1}$),

$$P = \frac{Q}{ATMP} = \frac{K}{\mu R} = \frac{K'}{R} \quad (S3)$$

thus, the permeation parameter, $K' = K/\mu$; here, for convenient comparison, the units of K and K' are

ignored. Then, the relation between water permeance and membrane thickness can be expressed as

Equation S4:

$$\text{Log} \left(\frac{1}{P} \right) = \text{Log} R - \text{Log} K \quad (\text{S4})$$

MD simulations: models and methods

In this work, the geometric structures of the MXene $\text{Ti}_3\text{C}_2\text{T}_x$ structure had been used in materials project database. Therefore, the MXene $\text{Ti}_3\text{C}_2\text{T}_x$ nanonanosheets had been determined by crystal structure of $\text{Ti}_3\text{C}_2\text{T}_x$. The Lennard-Jones (LJ) Potential function had been employed to calculate our systems. In our simulation, a number of water (H_2O) molecules were placed in the MXene $\text{Ti}_3\text{C}_2\text{T}_x$ between two nanonanosheets. The size of MXene nanonanosheet was $7.39\text{nm} \times 3.85\text{nm}$ (along x-y direction) in the primary simulation box, and a periodic boundary condition was applied. In addition, the other models is multi-walled carbon nanotubes (CNT) are embedded into MXene $\text{Ti}_3\text{C}_2\text{T}_x$. between layers. To obtain a global minimum energy configuration, a geometry optimization is first performed using the method of steepest-descent energy minimization with a convergence criteria of 0.00001 kcal/mol. The two unit cells are then allowed to equilibrate over NVT simulations (isothermal-isobaric ensemble) at a room temperature of 300 K and atmospheric pressure of 101 KPa for 20 ns with a time step of 1 fs. The requilibration molecular systems of the pure polymer matrix and tetranuclear complex can be obtained after a geometry optimization. These simulation processes are aimed to remove internal stresses in the polymer matrix. In addition, the adsorption energy between MXene $\text{Ti}_3\text{C}_2\text{T}_x$ nanosheet and H_2O molecules was calculated by considering the summary of short-range interactions and LJ interactions at last 5ns simulation. The molecules considered are nearest with the surface of MXene nanosheet. The diffusion coefficient (D) is calculated by mean square displacement, which has been obtained by the dynamic simulations.

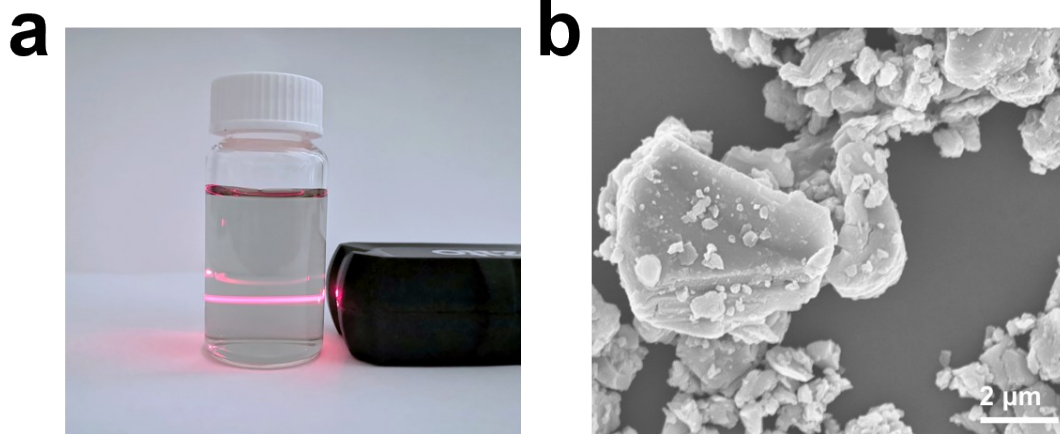


Fig. S1. (a) Photography of $\text{Ti}_3\text{C}_2\text{T}_x$ nanosheets dispersion showing the Tyndall scattering effect. (b) SEM images of Ti_3AlC_2 particles showing a typical brick-like structure with tightly stacked layers.

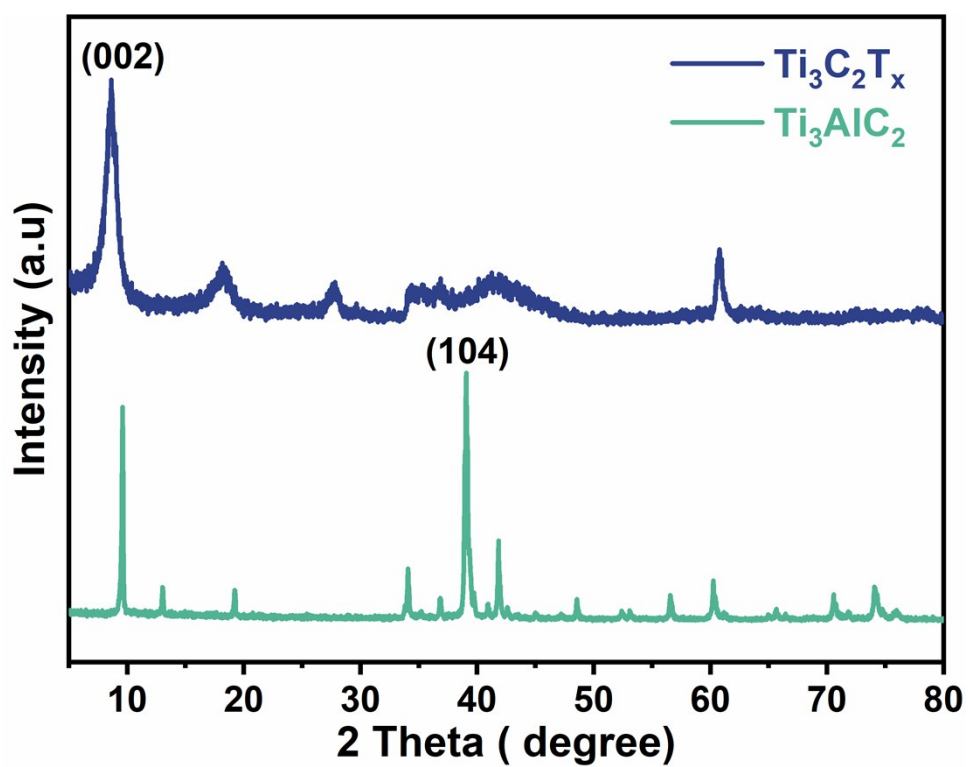


Fig. S2. XRD pattern of $\text{Ti}_3\text{C}_2\text{T}_x$ nanosheets and Ti_3AlC_2 particles

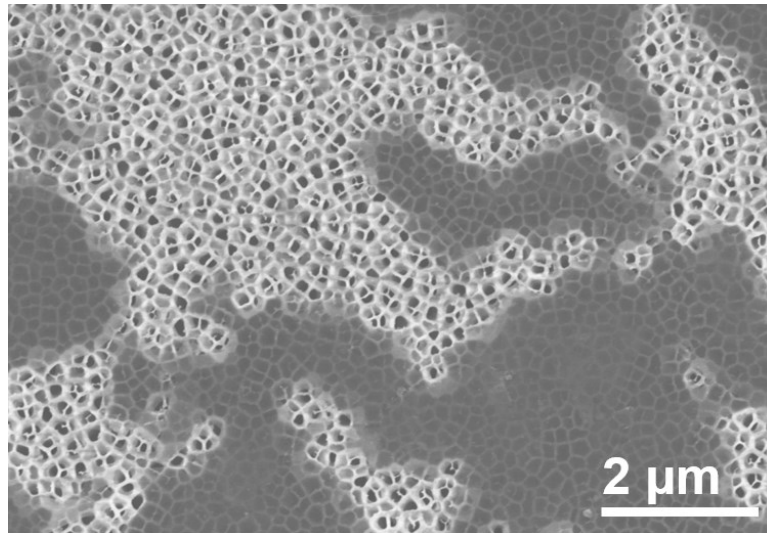


Fig. S3. SEM image for large scale $\text{Ti}_3\text{C}_2\text{T}_x$ nanosheets

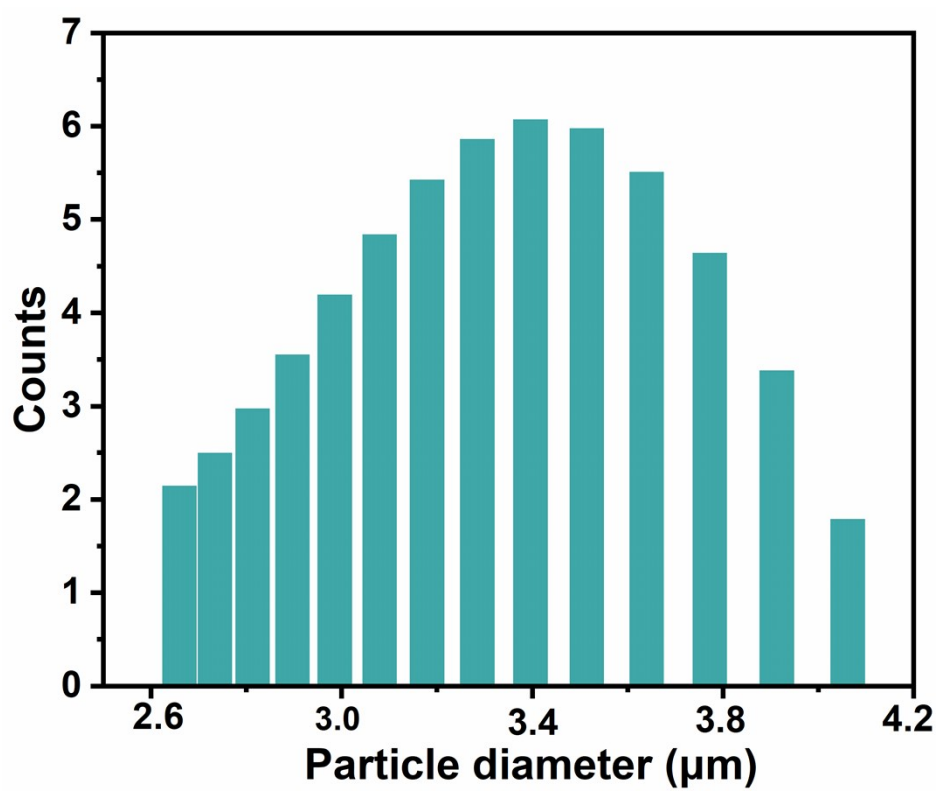


Fig. S4. Frequency histograms of $\text{Ti}_3\text{C}_2\text{T}_x$ lateral size.

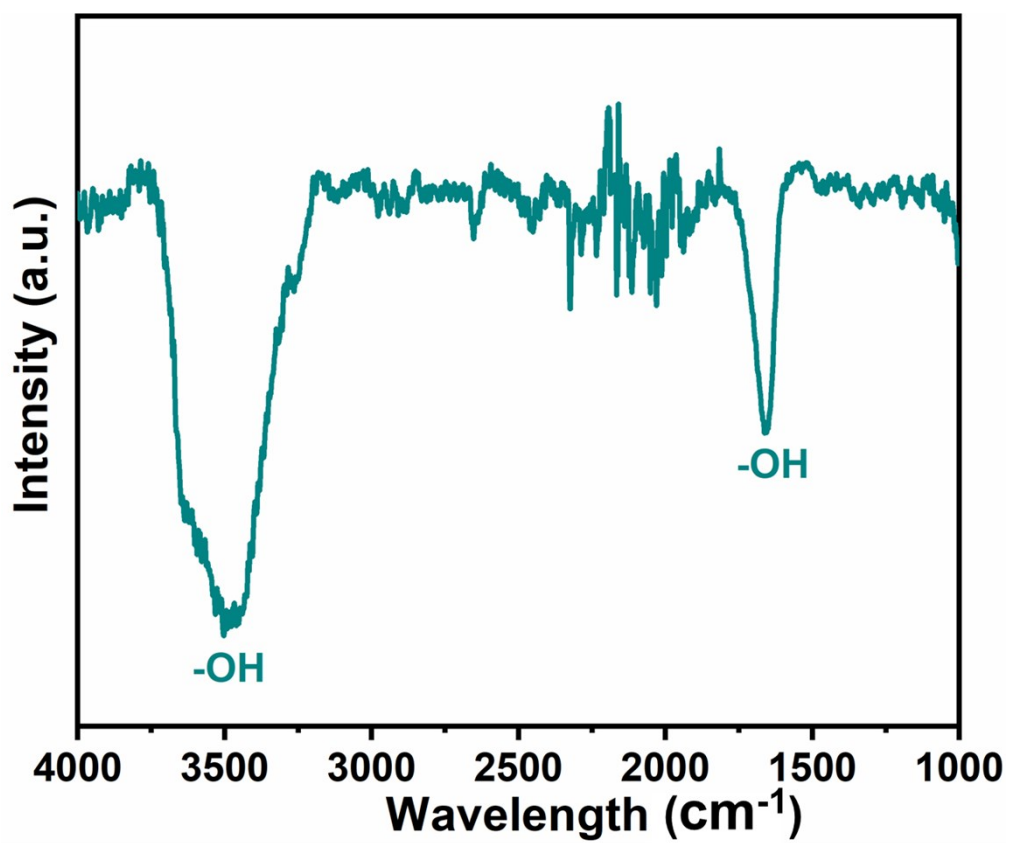


Fig. S5. FTIR spectra for $\text{Ti}_3\text{C}_2\text{T}_x$ nanosheets.

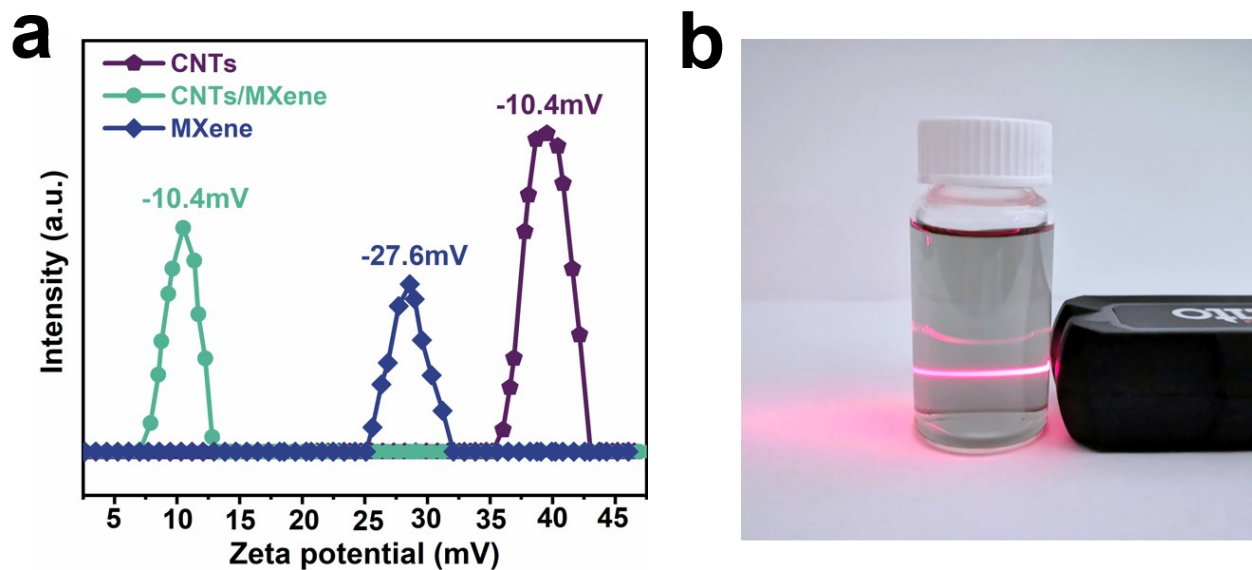


Fig. S6. (a) Zeta potential of CNTs, MXene and CNTs/MXene mixture. (b) Photography of MWCNTs/MXene mixture showing uniform dispersion with the Tyndall scattering effect.

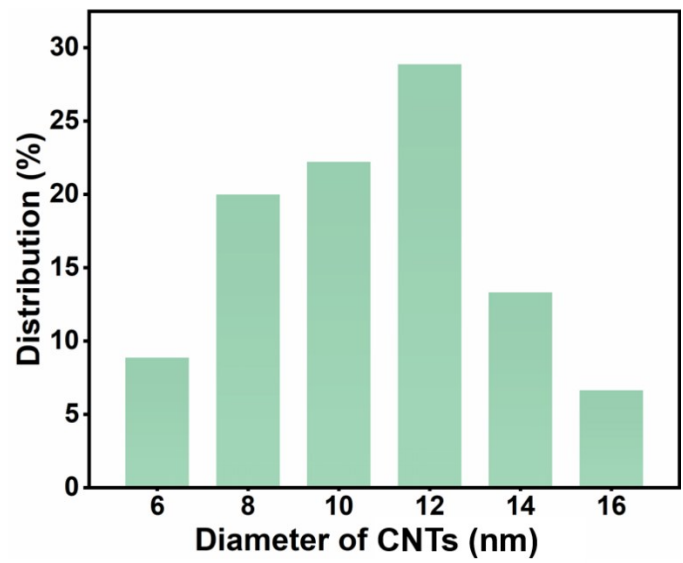
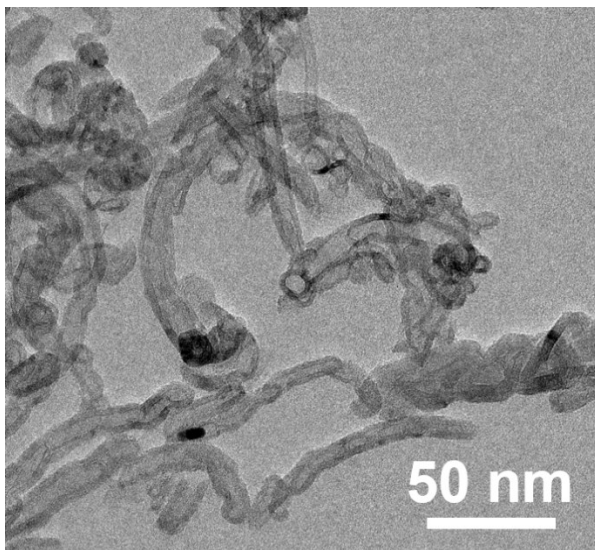


Fig. S7. TEM images and the diameter distribution profiles of the CNTs.

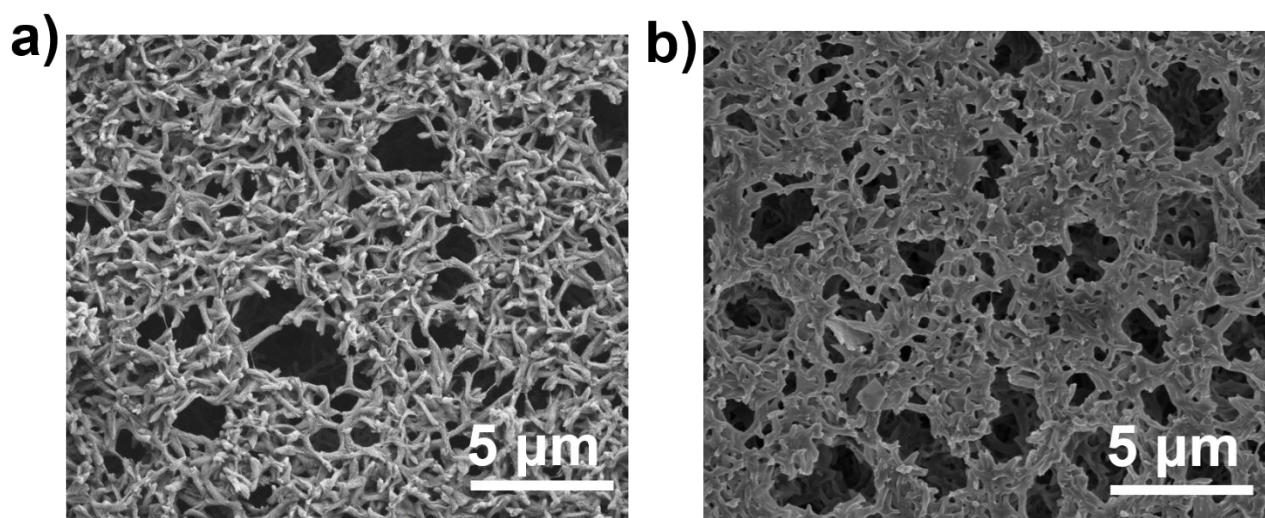


Fig. S8. SEM images of (a) pure Nylon substrate and (b) NaOH pre-treated Nylon substrate. It is found that the surface of Nylon substrate becomes smoother after NaOH treating, which is in favor of the uniform sheet deposition with ordered stacking.

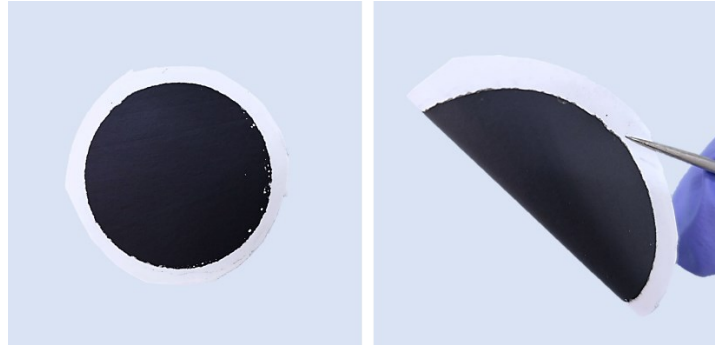


Fig. S9. Digital photography of 45%CNT-MX membrane with excellent flexibility.

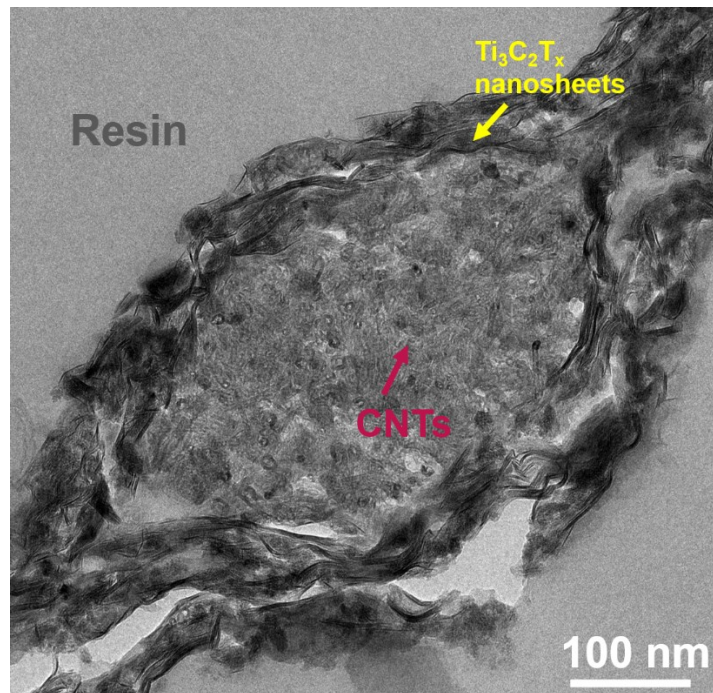


Fig10. TEM image of the cross-sectional view of the 45%CNT-MX membrane, showing distinct fusiform structure.

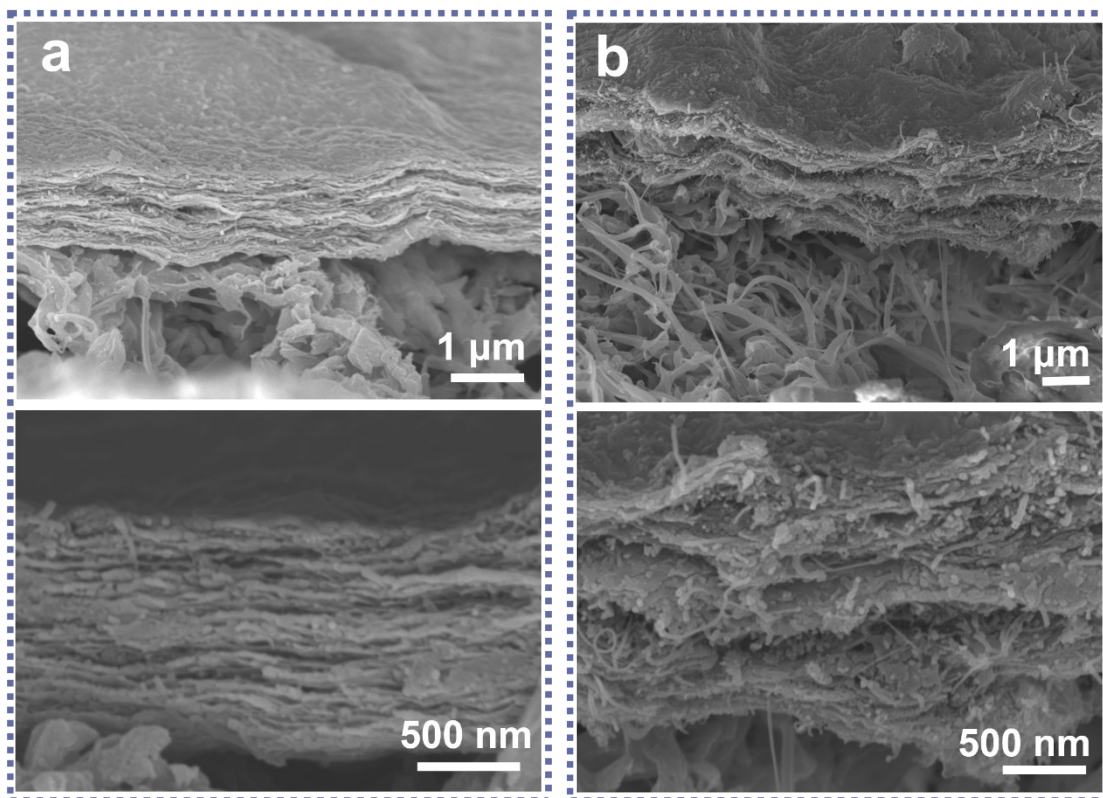


Fig. S11. FESEM images of the cross-sectional view of (a) 25%CNT-MX and (b) 60%CNT-MX membranes.

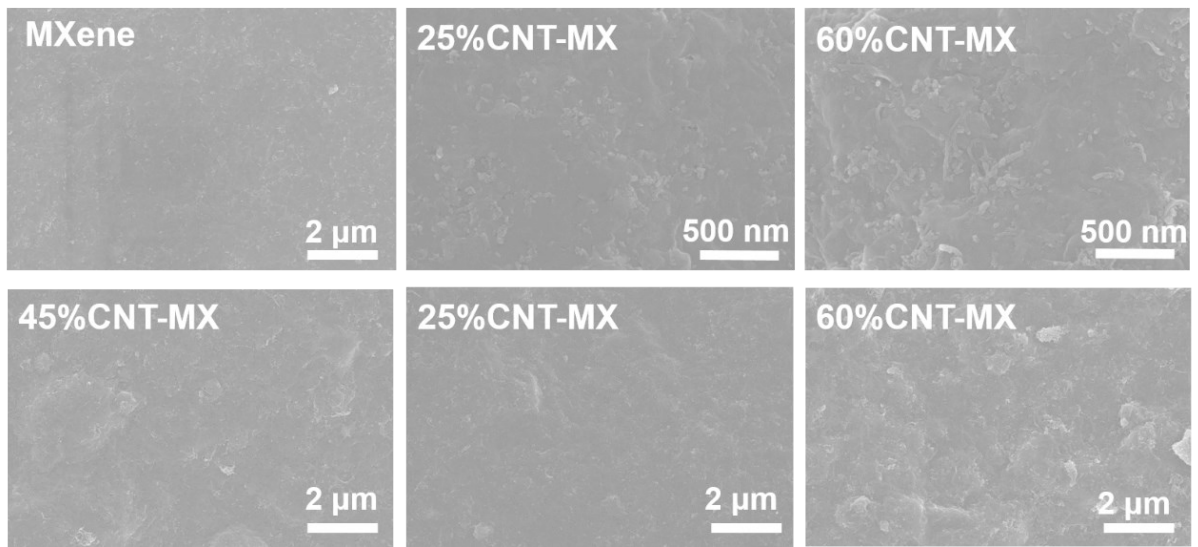


Fig. S12. FESEM images of surface views for membranes.

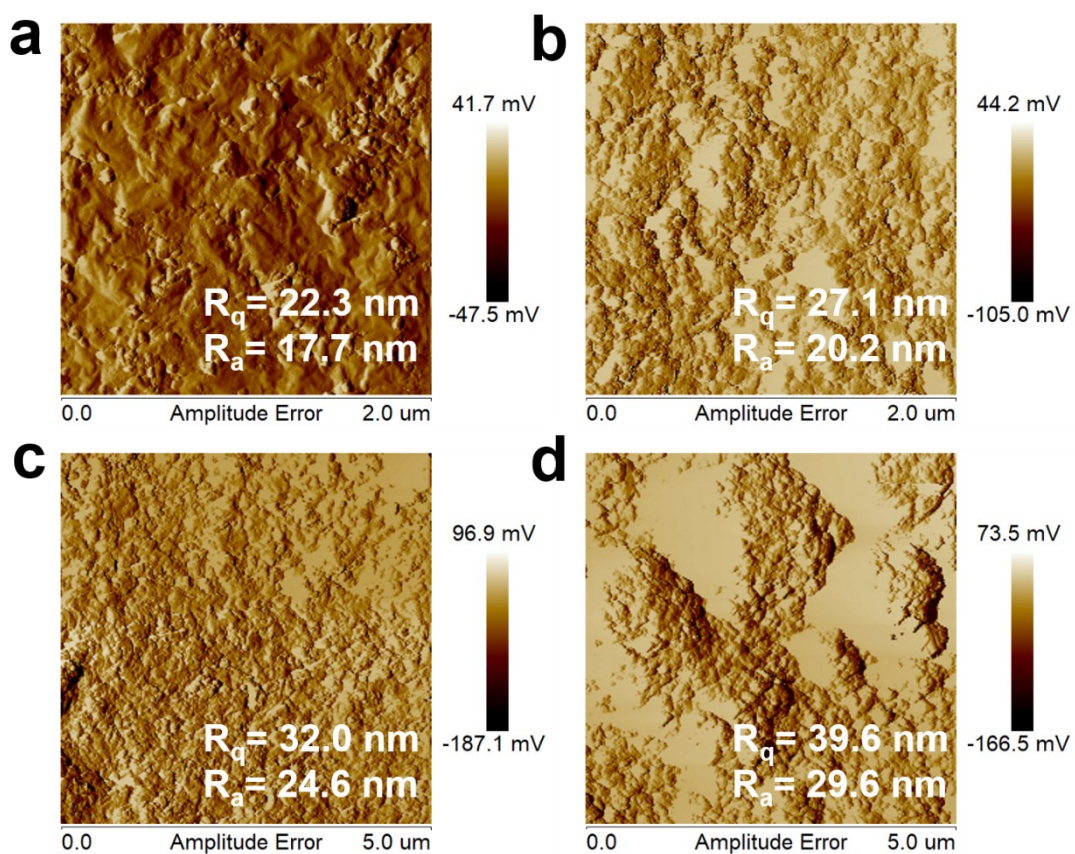


Fig. S13. AFM images for (a) pure MXene, (b) 25%CNT-MX, (c) 45%CNT-MX and (d) 60%CNT-MX membranes, respectively.

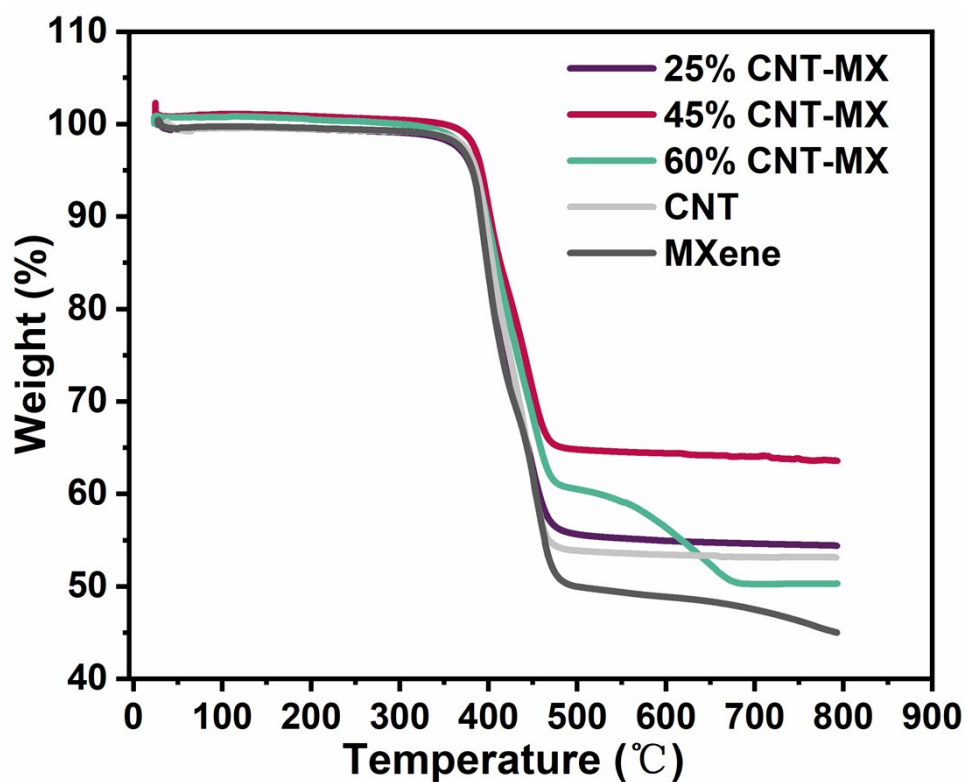


Fig. S14. The TGA curves of various membranes.

The weight loss occurring at about 350-460 °C is ascribed to the pyrolysis of the oxygen-containing functional groups that produce CO₂ and other gases. It is noticeable that the CNT-MX membranes show a low degree of weight loss except 60% CNT-MX, suggesting the excellent thermal stability, which might be due to the consume of oxygen-containing functional groups during fabrication process and the stronger interaction of interactions of hydrogen bonds between MXene nanosheets and CNTs. As for 60% CNT-MX, the higher weight loss is mainly due to the structure damage by the overloading CNTs.

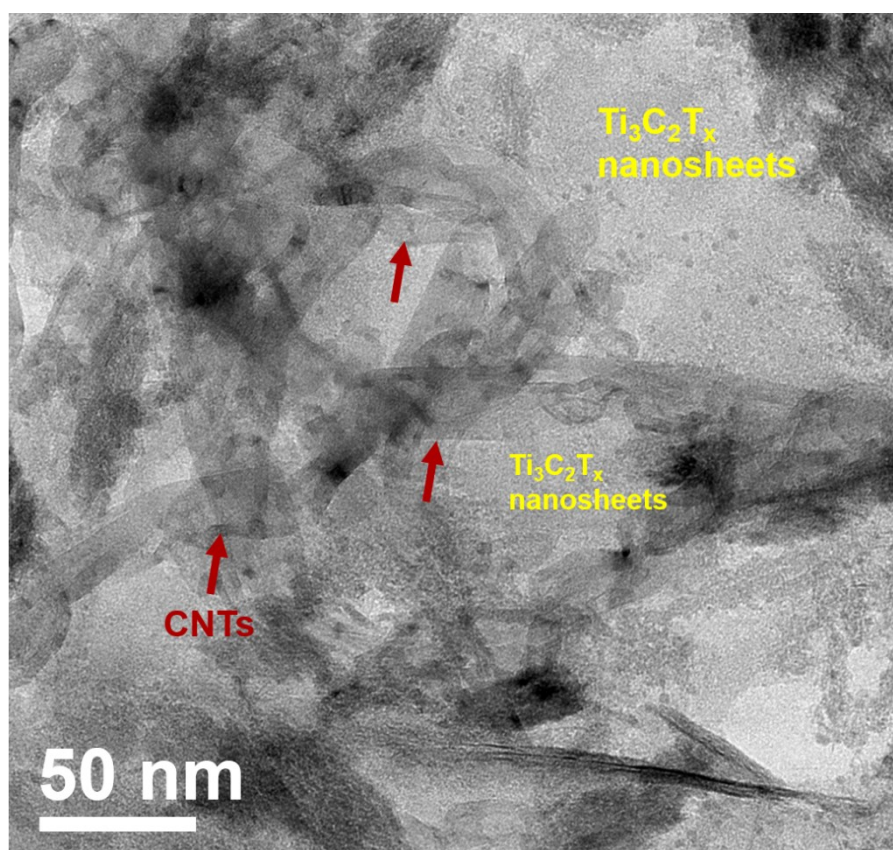


Fig. S15. TEM images of of top-sectional views for 45%CNT-MX membrane.

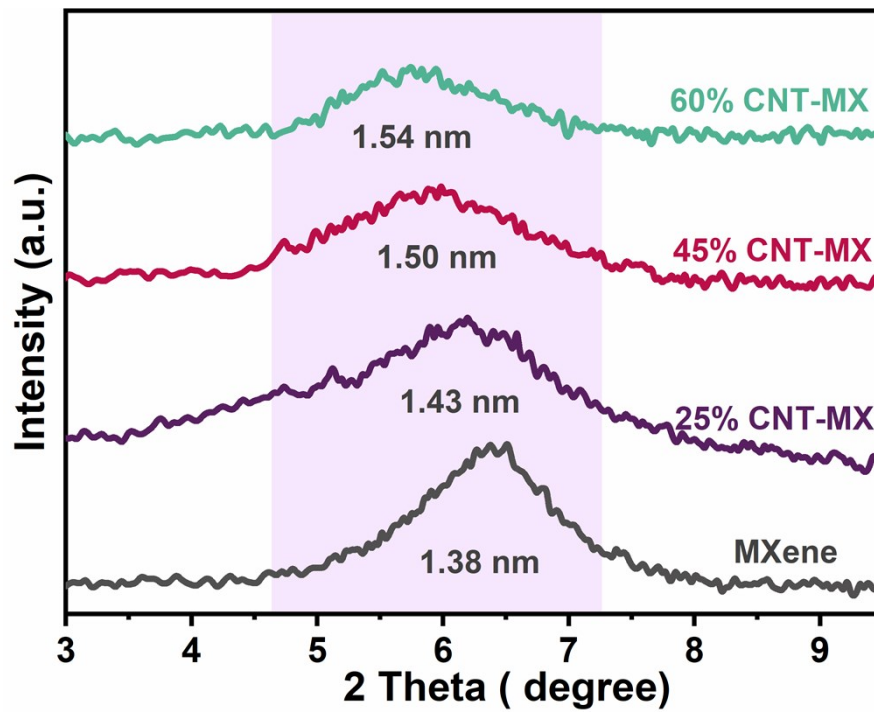


Fig. S16. XRD pattern of pure MXene and CNT-MX membranes.

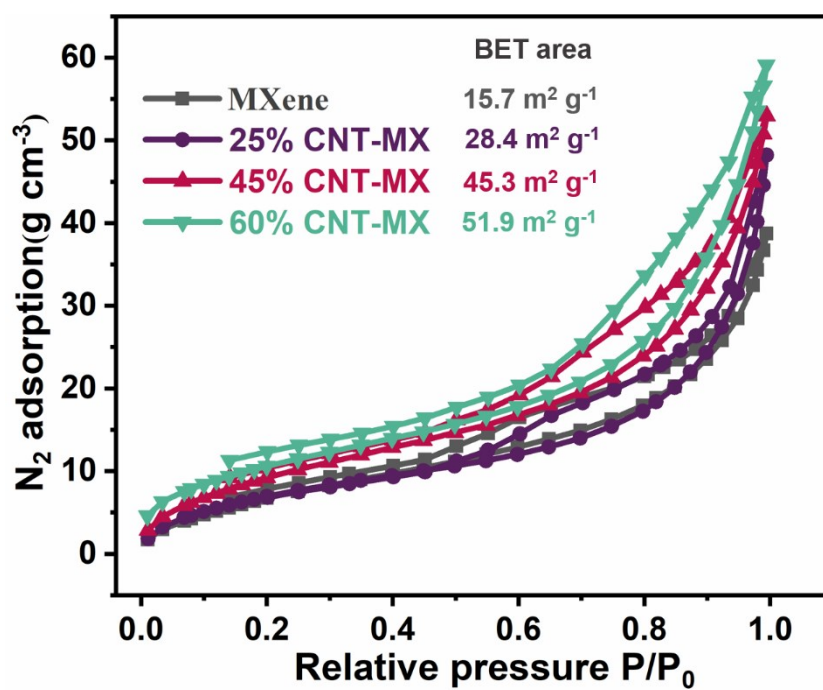


Fig. S17. N₂ adsorption-desorption isotherms of pure MXene, 25% CNT-MX, 45% CNT-MX and 60% CNT-MX membranes at 333 K, respectively.

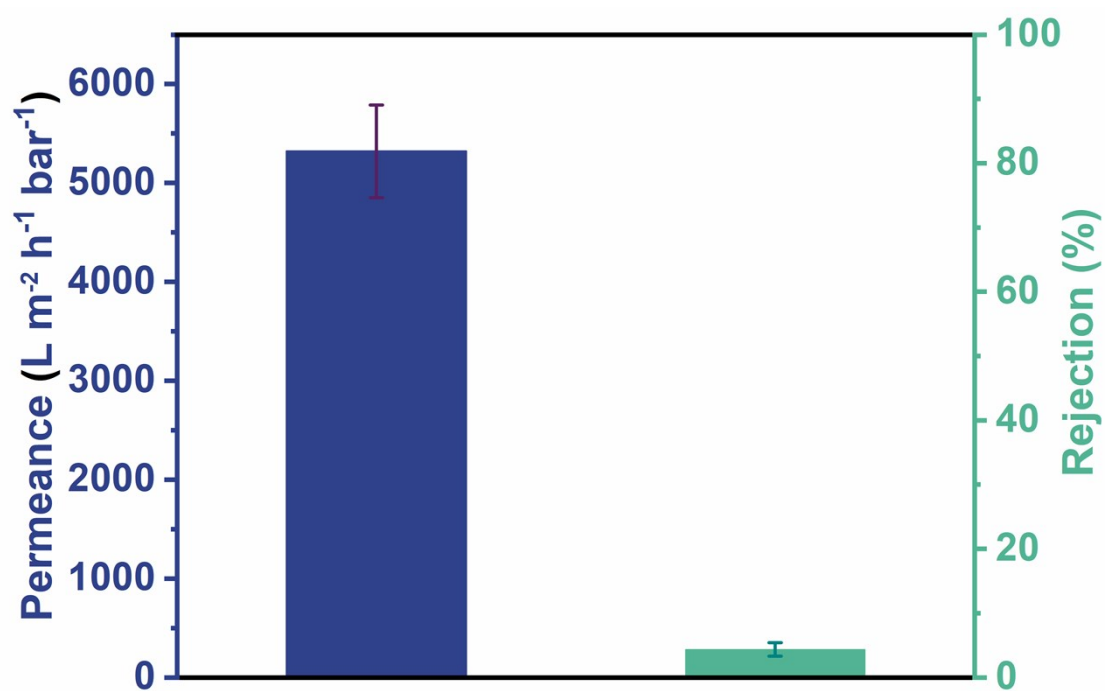


Fig. S18. Water permeance and rejection rates of CV for NaOH treated Nylon membrane.

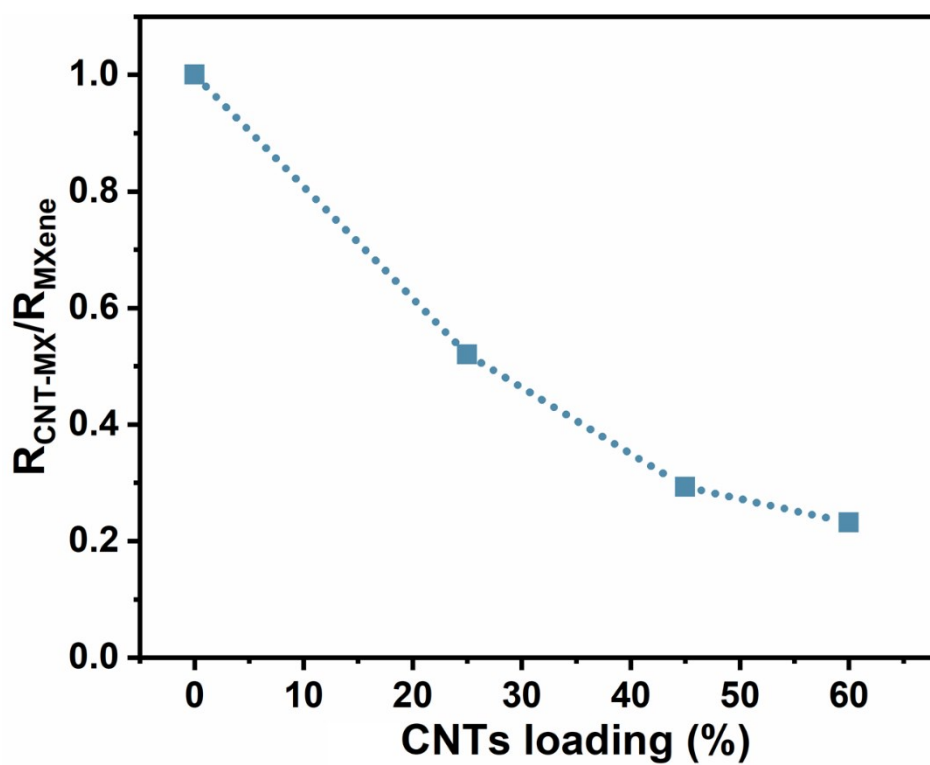


Fig. S19. Hydrodynamic resistance of the heterostructured CNT-MX membrane with diverse CNTs loadings normalized by that of the pure MXene membrane.

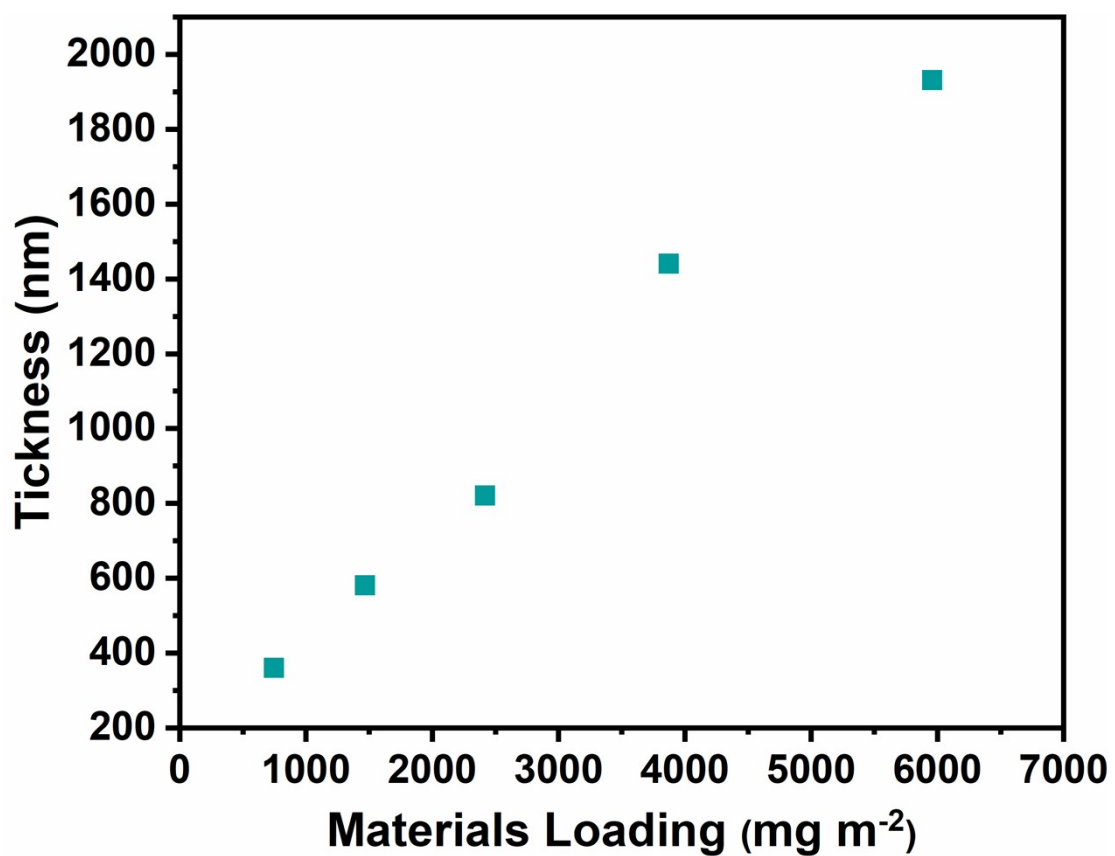


Fig. S20. Plot of membrane thickness vs materials loading, showing a practically linear relationship.

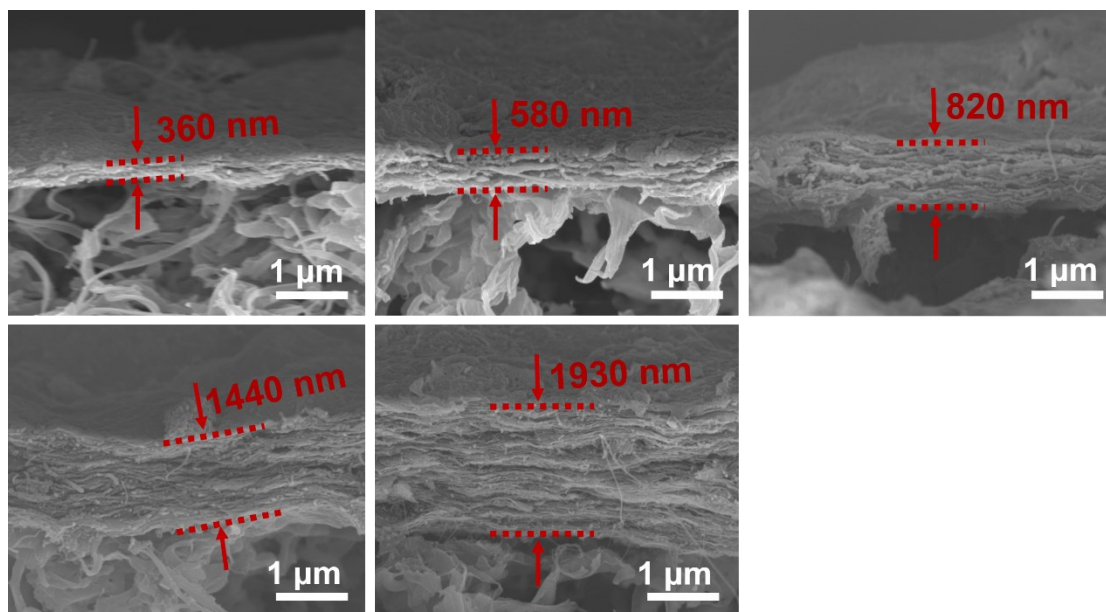


Fig. S21. FESEM images of cross-sectional view of 45% CNT-MX membranes with different thickness.

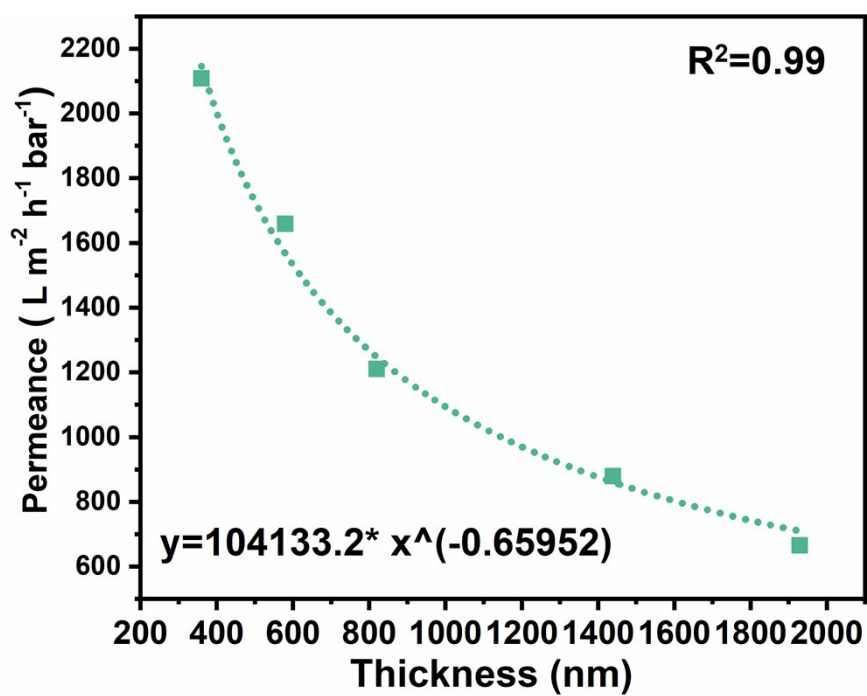


Fig. S22. Variation of the water permeance as a function of the membrane thickness. The pressure applied here was 1 bar.

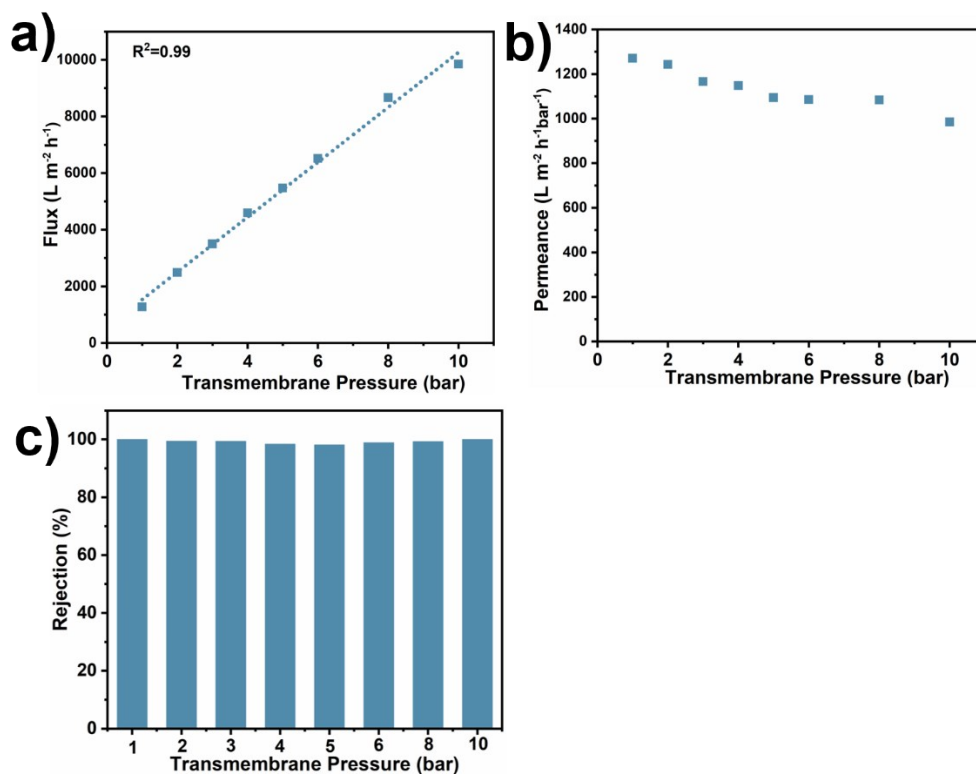


Fig. S23. a) Water flux, b) permeance and c) rejection rate of CV with applied pressure for the 45%CNT-MX membranes.

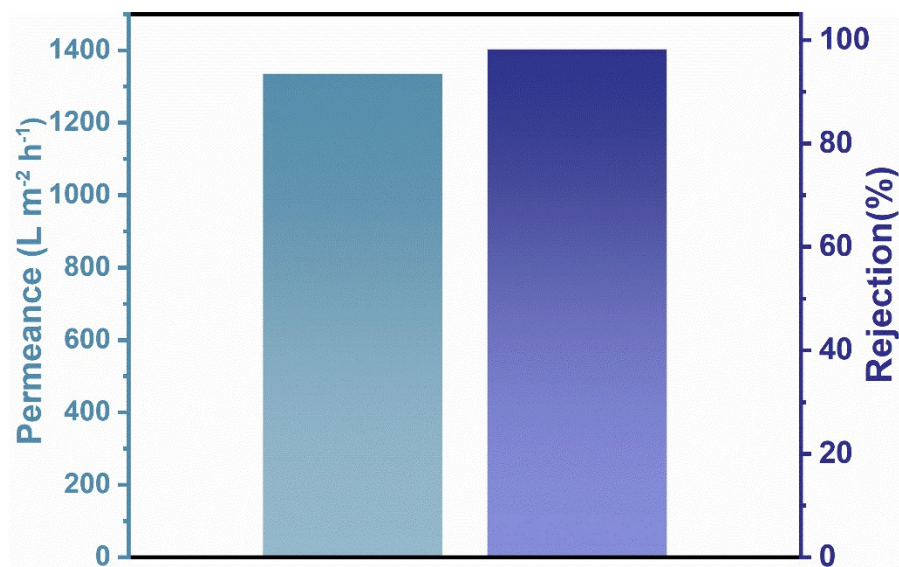


Fig. S24. Separation performance of 45%CNT-MX membranes for CV feed solution after immersing into in aqueous solution for 30 h.

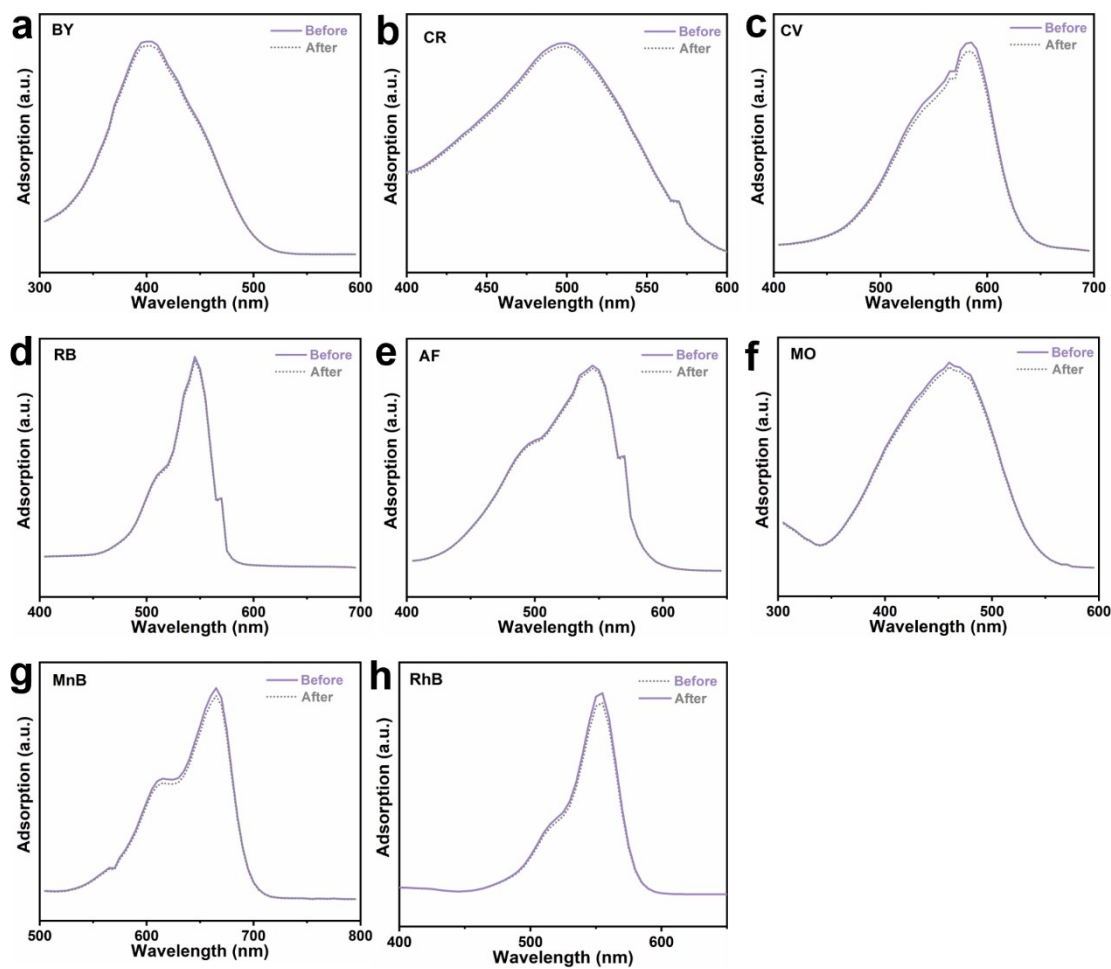


Fig. S25. UV-vis absorption spectra of various dyes before and after using 45% CNT-MX membranes immerse for 3 hours

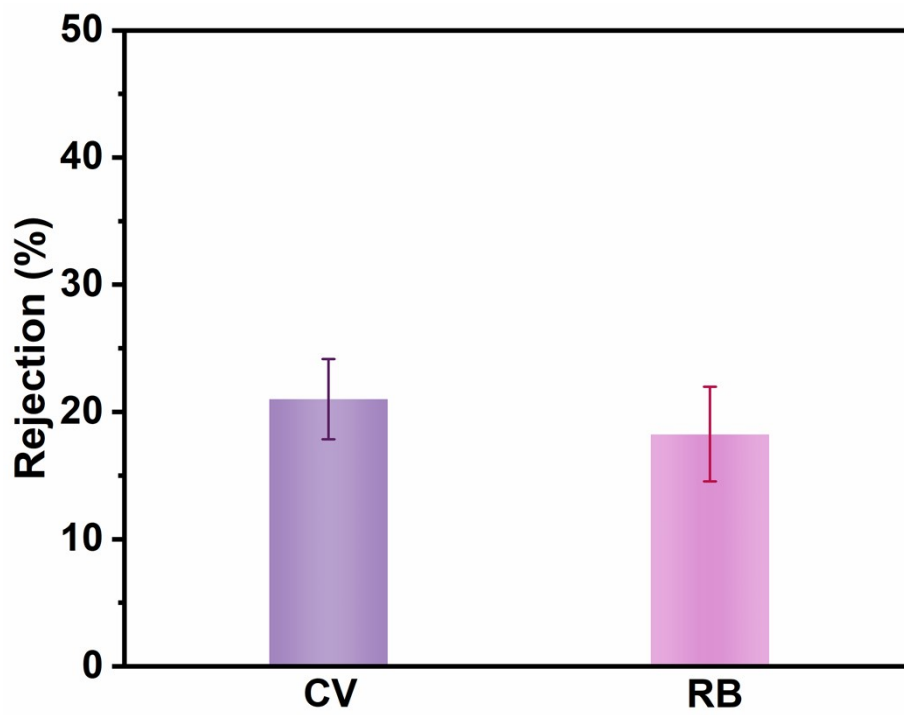


Fig. S26. Rejection rate of CV and RB for pure CNTs membrane.

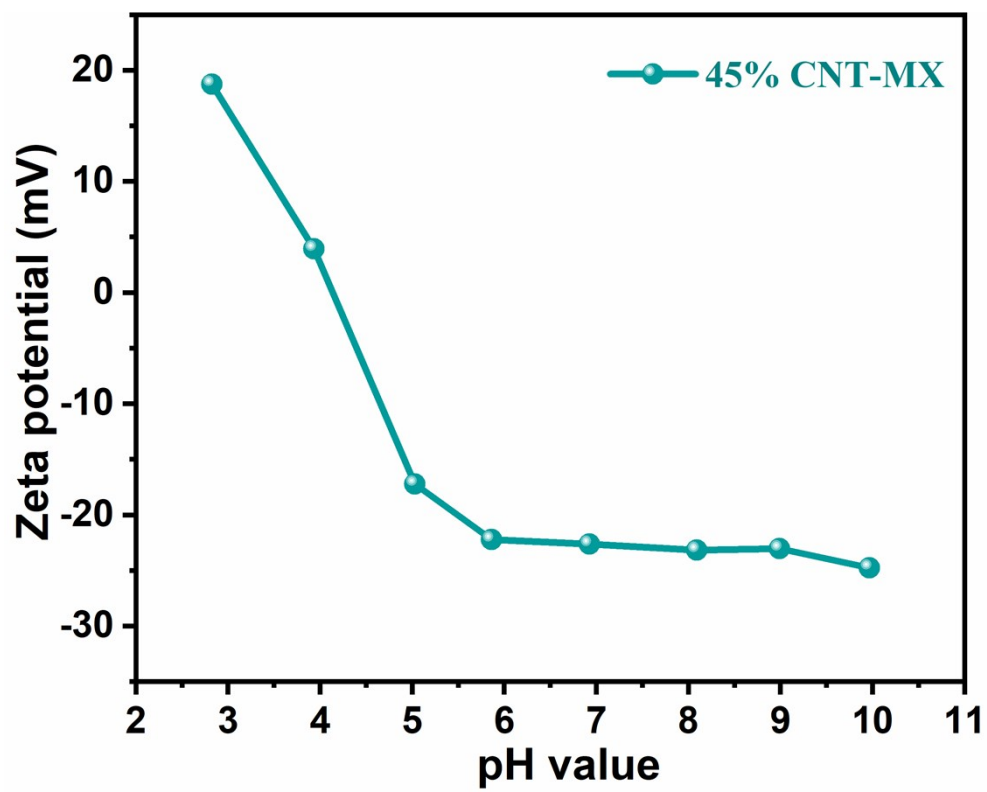


Fig. S27. Zeta potential for 45% CNT-MX membrane with the variation of pH value.

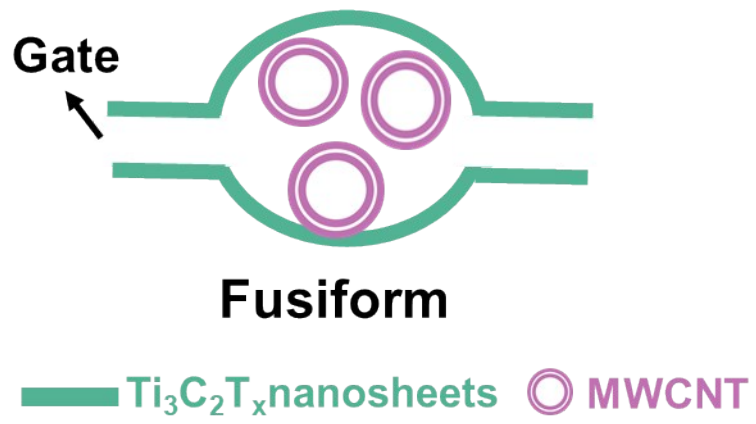


Fig. S28. Schematic illustration for the structure of the transport channels.

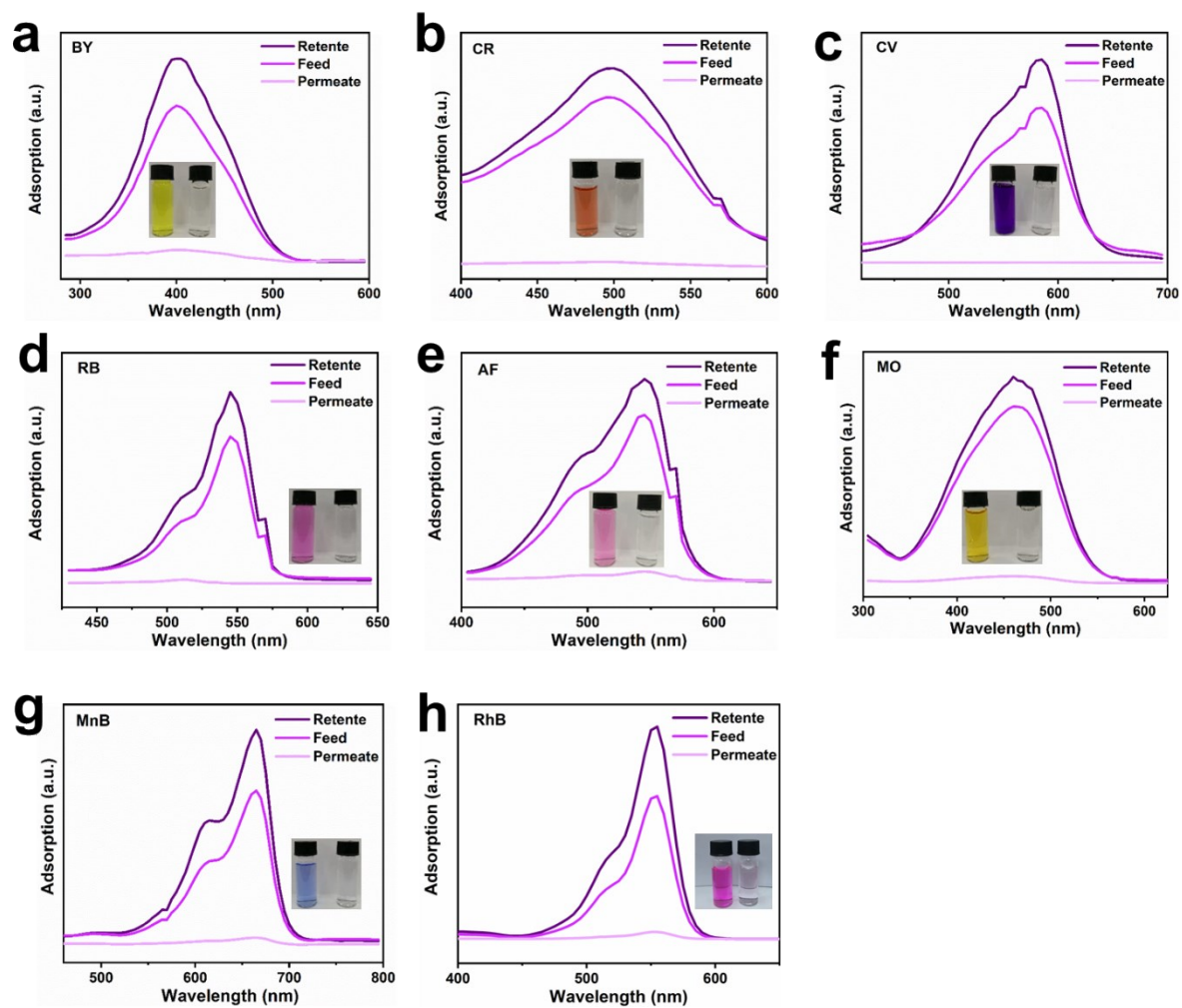


Fig. S29. UV-vis absorption spectra of the feed, the permeate and the retentate of a) BY, b) CR, c) CV, d) RB, e) AF, f) MO, g) MnB and h) RhB solution after filtration by 45% CNT-MX membrane.

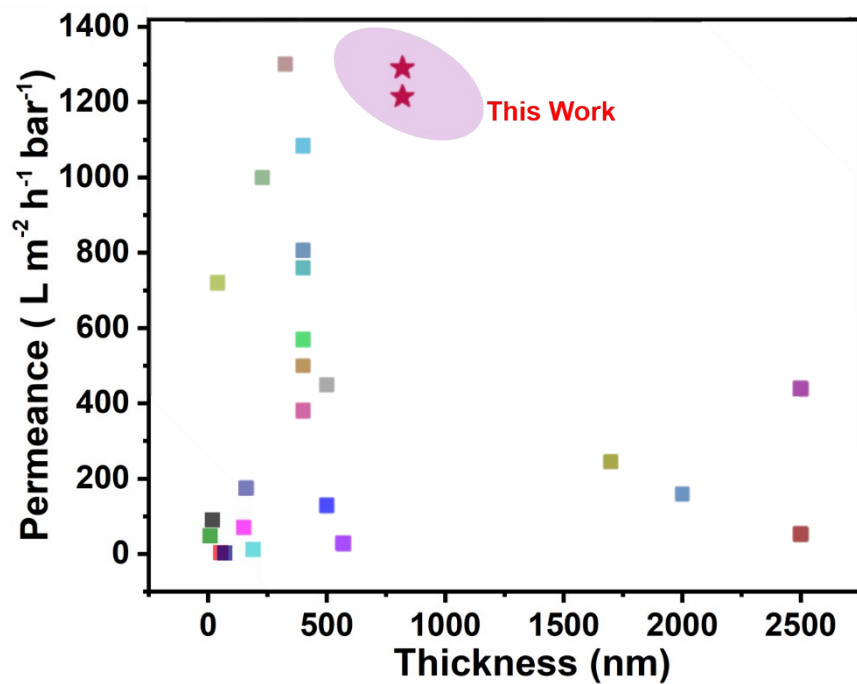


Fig. S30. Comparison of separation performance between 45% CNT-MX and various previously reported membranes. Detailed information about those membranes are listed in Table S2

Table S1. The chemical structures, molar weights and dimensional parameters of various dyes.

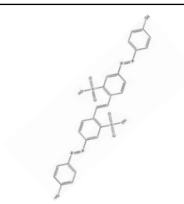
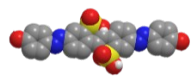
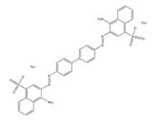
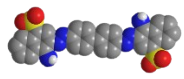
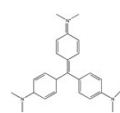
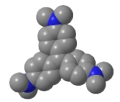
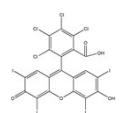

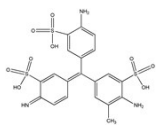
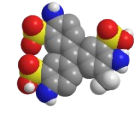
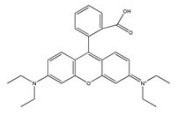
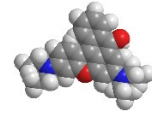
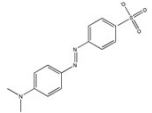
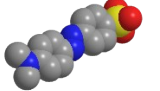
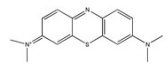
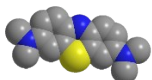
Dyes	Mw (g/mol)	Chemical structure	3D molecule structure	Dimension (nm)	Electrical property
Brilliant Yellow (BY)	625.6			2.6 ⁴	—
Congo Red (CR)	696.7			2.56 x 0.73 ⁵	—
Crystal Violet (CV)	408			2.0 ⁴	+
Rose Bengal (RB)	1017.6			1.2 x 1.54 ⁶	—
Acid Fuchsin (AF)	585.5			1.9 ⁴	—
Rhodamine B (RdB)	479.0			1.4 x 1.8 ⁷	—
Methyl Orange (MO)	327.3			1.13 x 0.42 ⁵	—
Methylene Blue (MnB)	373.9			1.25 x 0.51 ⁵	+

Table S2. Comparison of the separation performance for various membranes

Membrane	Thickness (nm)	Solute	Size (nm)	Rejection (%)	Water permeation (L m ² h ⁻¹ bar ⁻¹)	Reference
S-rGO-18	18	EB	3.1	100	90.2	4
uGNMs(GO)	53	MnB	1.5	99.8	3.26	8
GO-RF8	500	MnB	1.5	94	130	9
Shear-aligned GO	150	MnB	1.5	99.5	71	10
HLGO	8	MnB	1.5	95.5	48	11
GO	70	MnB	1.5	96	2.8	11
RGO- MWCNT(50)	570	MnB	1.5	95	28	12
CDs-GO/MCE	2500	MnB	1.5	94.1	439	12
GO	2500	MnB	1.5	99.9	53	13
MoS ₂ membrane	1700	EB	3.1	90	245	14
MoS ₂ membrane	2000	EB	3.1	90	160	
COF-LZU1	400	MnB	1.5	99	760	5
COF-LZU1	400	MnB	1.5	99	500	5
COF-LZU1	400	AF	1.7	91.4	570	5
COF-LZU1	400	rhB	1.8	99	380	5
g-C ₃ N ₄ membrane	190	rhB	1.8	90	11.9	15
SWCNT- intercalated GO	160	rhB	1.8	99	175	16
SWCNT- intercalated GO	40	rhB	1.8	97.4	720	16
WS ₂ membrane	500	EB	3.1	93	450	17

Ti ₃ C ₂ T _x -C ₁₂ H ₂₅	324	MO	1.2	35	1300	18
Ti ₃ C ₂ T _x -NH ₂	300	MO	1.2	73	1563	18
Ti ₃ C ₂ T _x -C ₁₂ H ₂₅	300	MnB	1.5	92	1563	18
MXene (wet)	200	AY79	2.8	96.3	2302	19
MXene (wet)	230	AY14	1.9	55	1000	19
MXene (dry)	200	AY79	2.8	98.6	1703	19
MXene	400	EB	3.1	90	1084	20
Mxenne	400	rhB	1.8	85	806	20
CNT-MX	820	CV	2	99.8	1214.3	This work
CNT-MX	820	MO	1.2	95.3	1290.5	This work

References

1. Chou, S. Shi, L. Wang, R. Tang, C. Y. Qiu, C. Fane, A. G. *Desalination* 2010, **261**, 365-372.
2. Fang, H. H. P. Shi, X. *J. Membr. Sci.*, 2005, **264**, 161-166.
3. Boateng, L. K. Madarshahian, R. Yoon, Y. Caicedo, J. M. Flora, J. R. *J. Mol. Model.*, 2016, **22**, 185.
4. Huang, L. Chen, J. Gao, T. Zhang, M. Li, Y. Dai, L. Qu, L. Shi, G. *Adv. Mater.*, 2016, **28**, 8669-8674.
5. Fan, H. Gu, J. Meng, H. Knebel, A. Caro, J. *Angew. Chem. Int. Ed.*, 2018, **57**, 4083-4087.
6. Kandambeth, S.; Biswal, B. P.; Chaudhari, H. D.; Rout, K. C.; Kunjattu, H. S.; Mitra, S.; Karak, S.; Das, A.; Mukherjee, R.; Kharul, U. K.; Banerjee, R. *Adv. Mater.* 2017, **29**.
7. Huang, H.; Song, Z.; Wei, N.; Shi, L.; Mao, Y.; Ying, Y.; Sun, L.; Xu, Z.; Peng, X., *Nat. Commun.*, 2013, **4**, 2979.
8. Han, Y. Xu, Z. Gao, C. *Adv. Funct. Mater.*, 2013, **23**, 3693-3700.
9. Lee, C. S. Choi, M. K. Hwang, Y. Y. Kim, H.; Kim, M. K. Lee, Y. J. *Adv. Mater.*, 2018, **30** , e1705944.
10. Akbari, A. Sheath, P. Martin, S. T. Shinde, D. B. Shaibani, M. Banerjee, P. C. Tkacz, R. Bhattacharyya, D. Majumder, M. *Nat. Commun.* 2016, **7**, 10891.
11. Yang, Q. Su, Y. Chi, C. Cherian, C. T. Huang, K. Kravets, V. G. Wang, F. C. Zhang, J. C. Pratt, A. Grigorenko, A. N. Guinea, F. Geim, A. K. Nair, R. R. *Nat. Mater.*, 2017, **16**, 1198-1202.
12. Goh, K. Jiang, W. Karahan, H. E. Zhai, S. Wei, L. Yu, D. Fane, A. G. Wang, R.; Chen, Y. *Adv. Funct. Mater.*, 2015, **25**, 7348-7359.
13. Wang, W. Eftekhari, E. Zhu, G. Zhang, X. Yan, Z. Li, Q. *Chem. Commun.*, 2014, **50**, 13089-92.
14. Sun, L. Huang, H. Peng, X. *Chem. Commun.*, 2013, **49**, 10718-20.
15. Wang, Y. Li, L. Wei, Y. Xue, J. Chen, H. Ding, L. Caro, J. Wang, H. *Angew. Chem. Int. Ed.*, **2017**, **56**, 8974-8980.
16. Gao, S. J. Qin, H. Liu, P. Jin, J. *J. Mater. Chem. A* 2015, **3**, 6649-6654.
17. Sun, L. Ying, Y. Huang, H. Song, Z. Mao, Y. Xu, Z. Peng, X. *ACS Nano* 2014, **8**, 6304-6311.
18. Wu, X. Cui, X. Wu, W. Wang, J. Li, Y. Jiang, Z. *Angew. Chem. Int. Ed.*, 2019, **58**, 18524-18529.
19. Wang, J. Chen, P. Shi, B. Guo, W. Jaroniec, M. Qiao, S. Z. *Angew. Chem. Int. Ed.*, 2018, **57**, 6814-6818.

20. Ding, L. Wei, Y. Wang, Y. Chen, H. Caro, J. Wang, H. *Angew. Chem. Int. Ed.*, 2017, **56**, 1825-1829.